This is the accepted manuscript made available via CHORUS. The article has been published as:

Resolved Atomic Interaction Sidebands in an Optical Clock Transition

M. Bishof, Y. Lin, M. D. Swallows, A. V. Gorshkov, J. Ye, and A. M. Rey

Resolved atomic interaction sidebands in an optical clock transition

M. Bishof[1], Y. Lin[1], M. D. Swallows[1], A. V. Gorshkov[2], J. Ye[1] and A. M. Rey[1]

[1] *JILA and Department of Physics, NIST and University of Colorado, Boulder, CO 80309-0440, USA and*
[2] *Institute for Quantum Information, California Institute of Technology, Pasadena, CA 91125, USA*

We report the observation of resolved atomic interaction sidebands (ISB) in the ^{87}Sr optical clock transition when atoms at microkelvin temperatures are confined in a two-dimensional (2D) optical lattice. The ISB are a manifestation of the strong interactions that occur between atoms confined in a quasi-one-dimensional geometry and disappear when the confinement is relaxed along one dimension. The emergence of ISB is linked to the recently observed suppression of collisional frequency shifts in [1]. At the current temperatures, the ISB can be resolved but are broad. At lower temperatures, ISB are predicted to be substantially narrower and usable as powerful spectroscopic tools in strongly interacting alkaline-earth gases.

Experimental efforts in control of ultracold alkaline-earth atoms (AEA), such as Sr or Yb, have led to remarkable developments in optical atomic clocks [1, 2], which are approaching the accuracy of single ion standards [3]. Fermionic AEA are also attracting considerable attention in the context of quantum information science [4–6]. Many of these applications require reaching the strongly interacting regime, in which interactions dominate over all relevant dynamical energy scales. In this Letter, we demonstrate the onset of strong interactions in a low dimensional gas of ^{87}Sr atoms by observing resolved interaction sidebands (ISB) in Rabi spectroscopy of the $^1S_0 - {}^3P_0$ optical clock transition.

Rabi spectroscopy has served as an excellent probe for interacting alkali gases. For example, it was used to detect and characterize Bose Einstein condensation in spin polarized hydrogen [7], to measure the fermion pair wave function in the BEC-BCS crossover [8], and to resolve the Mott insulator shell structure in a bosonic lattice system [9]. Here, we show that the ISB that emerge during optical Rabi interrogation can become a powerful spectroscopy tool to uniquely probe lattice-trapped AEA. At microkelvin temperatures and loading conditions of mainly one or two atoms per lattice site, we observe a single ISB, which can be resolved from the carrier but is broad. However, in the quantum degenerate regime, the ISB are expected to become substantially narrower and could thus lead to a precise determination of the s-wave $^1S_0 - {}^3P_0$ interaction parameters that remain unknown. We also show that the variation in ISB spectra between sites with different numbers of atoms allows for a precise characterization of atom number occupations in interacting AEA systems.

When the $^1S_0$ and $^3P_0$ electronic degrees of freedom within a single atom are represented as an effective pseudo-spin 1/2 (g and e), two nuclear-spin polarized atoms form a simple model for understanding the appearance of ISB (Fig. 1). We consider atoms trapped in a tube geometry with a weak trapping frequency ω_Z along $\hat{Z}$ and a strong transverse confinement $\hbar\omega_{X,Y} \gg k_B T_{X,Y}$, large enough to forbid any transverse dynamics [$T_X(T_Y)$ is the temperature along $\hat{X}(\hat{Y})$]. We assume the atoms are prepared in the same pseudo-spin state ($|gg\rangle$) and interrogated by a linearly polarized laser beam with bare Rabi frequency Ω^B and detuning from the atomic resonance δ. The Pauli exclusion principle forces atoms in
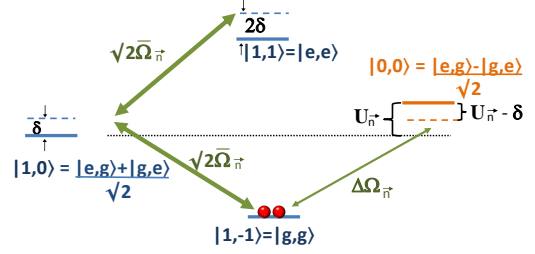

FIG. 1: (Color online) Schematic diagram of Rabi spectroscopy in the strongly interacting regime. When $\delta \approx 0$, only the non-interacting triplet states ($S = 1$) are accessible, giving rise to an interaction-free carrier. However, when $\delta \sim U_{\vec{n}}$, the singlet $|0,0\rangle$ becomes resonant, and a slightly inhomogeneous coupling ($\Delta\Omega_{\vec{n}} \neq 0$) can induce population transfer to it, as manifested in an ISB.

identical internal states to occupy different vibrational levels along $\hat{Z}$, $\vec{n} = (n_1, n_2)$, since their spatial wave function must be antisymmetric. Being identical fermions, the atoms initially experience zero s-wave interaction. If the atoms are coherently driven to e (i.e. if they experience the same Rabi frequency $\bar{\Omega}_{\vec{n}} \equiv (\Omega_{n_1} + \Omega_{n_2})/2$), then the effective spin must remain symmetric under exchange. Consequently, during the excitation the atoms will not experience any s-wave interactions. We refer to states with spin-symmetric wave functions, $|gg\rangle \equiv |S = 1, M = -1\rangle$, $|ee\rangle \equiv |1,1\rangle$ and $(|eg\rangle + |ge\rangle)/\sqrt{2} \equiv |1,0\rangle$, as the triplet states, $S = 1$ [10, 11].

However, in optical transitions, a small component of the probe beam along $\hat{Z}$ leads to a slightly different Rabi frequency $\Omega_{n_j}(\eta_Z^2)$ for each mode, with $\eta_Z = k_Z a_{ho}^Z / \sqrt{2}$ the Lamb-Dicke parameter, m the atom mass, k_Z the component of the probe laser wave vector along $\hat{Z}$ and $a_{ho}^Z = \sqrt{\frac{\hbar}{m\omega_Z}}$ the $\hat{Z}$ harmonic oscillator length. If $\Delta\Omega_{\vec{n}} = (\Omega_{n_1} - \Omega_{n_2})/\sqrt{2}$ is not zero, then the optical excitation-induced inhomogeneity can transfer some of the atoms to the antisymmetric pseudo-spin singlet state, $(|eg\rangle - |ge\rangle)/\sqrt{2} \equiv |0,0\rangle$. The interacting singlet is separated from $|1,0\rangle$ by an interaction energy $U_{\vec{n}}$.

In the limit where $\delta \sim \bar{\Omega}_{\vec{n}} \ll U_{\vec{n}}$, a small $\Delta\Omega_{\vec{n}}$ cannot overcome the energy cost required to drive the transition to the singlet (Fig. 1). Evolution into the singlet is blocked and the atoms remain non-interacting. However, if we increase the

detuning to $\delta \sim U_{\vec{n}}$, the transition $|1,-1\rangle \rightarrow |0,0\rangle$ becomes resonant. Here, a small $\Delta\Omega_{\vec{n}}$ can efficiently transfer the atoms to the singlet, giving rise to an ISB in the lineshape. If instead of preparing the atoms in g we prepare the atoms in e, the ISB occurs at $\delta \sim -U_{\vec{n}}$.

The ISB resemble motional sidebands that develop in spectroscopy of trapped ions when the trapping frequency is much larger than the recoil energy, the so called Lamb-Dicke regime [12]. In this case, the carrier becomes free of Doppler shifts up to the corresponding "Stark shift" [13], and all motional effects are manifested in the sidebands. In our case, the ISB are pushed away from the carrier due to the large energy separation between interacting and non-interacting states, leaving the carrier free from interaction effects, up to a correction proportional to $\Delta\Omega_{\vec{n}}^2/U_{\vec{n}}$. Operating our Sr lattice clock in the strongly interacting regime has allowed us to suppress the collisional frequency shift to the 10^{-17} level, as reported in Ref. [1]. The observation of ISB unambiguously confirms the connection between suppression of collisions and strong interactions. This further supports the prospect of operating neutral atom clocks with large atom numbers to achieve the highest possible stability and accuracy.

Our experiment employs nuclear spin-polarized ($m_I = +9/2$) ^{87}Sr atoms loaded in two lattice configurations: a one-dimensional (1D) vertical lattice which creates an array of quasi-two-dimensional traps (pancakes) along $\hat{Y}$ with weak confinement along the $\hat{X}$ and $\hat{Z}$ directions, and a deep 2D lattice which creates an array of quasi-1D traps (tubes) in the $\hat{X}$-$\hat{Y}$ plane and has weak confinement along $\hat{Z}$. To prepare the atomic system, we laser cool ^{87}Sr atoms to about 2 μK inside a magneto-optic trap based on the weak $^1S_0 - {}^3P_1$ transition and then load them into a 1D vertical lattice. The spatial distribution of occupied 1D lattice sites is determined by the vertical extent of the MOT cloud, which is approximately Gaussian with a standard deviation $\sigma_V = 30$ μm. For the 2D lattice confinement we then adiabatically ramp up the horizontal lattice (along $\hat{X}$). To remove any atoms trapped in the 1D vertical lattice outside the 2D intersection region, we ramp the vertical lattice off and then back on. The number of horizontal lattice sites occupied is determined by the radial temperature of the vertical lattice. Atoms load into $\sim$100 rows of tubes uniformly distributed along $\hat{Y}$, while the columns distributed along $\hat{X}$ are loaded according to a Gaussian distribution with standard deviation σ_H of 6-10 μm. After forming the lattices, we perform Doppler and sideband cooling using the $^1S_0 - {}^3P_1$, $F = 11/2$ transition. Simultaneously, atoms are optically pumped to the $m_I = +9/2$ ground state magnetic sublevel, using σ^+-polarized light on the $^1S_0 - {}^3P_1$, $F = 9/2$ transition, propagating along a bias magnetic field parallel to $\hat{Z}$. We perform spectroscopy of the $^1S_0 - {}^3P_0$ transition using a narrow linewidth laser propagating along $\hat{Y}$.

We quantify the number of atoms by detecting fluorescence on the strong $^1S_0 - {}^1P_1$ transition at 461 nm. Temperature and trap frequencies are extracted from Doppler spectroscopy along $\hat{Z}$ and vibrational sideband spectra [1, 14]. We estimate that we loaded $\sim$7000 atoms in the 1D lattice distributed in

$\sim$420 pancakes and $\sim$17 atoms per pancake. We determine $\omega_Y = 2\pi \times 80$ kHz and $\omega_{X,Z} = 2\pi \times 500$ Hz, and $T_{X,Y,Z} \sim 4$ μK. For the 2D lattice, we loaded $\sim$3000 atoms and $\sim 30\%$ of the populated tubes are doubly occupied. We determine $\omega_X = 2\pi \times 110$ kHz, $\omega_Y = 2\pi \times 70$ kHz and $\omega_Z = 2\pi \times 800$ Hz at trap center, and $T_{X,Y,Z} \sim 4.5$ μK.

ISB develop in the lineshape only in the parameter regime where $\gamma \equiv E_{\text{int}}/\langle\bar{\Omega}\rangle_T \gg 1$. Here, $E_{\text{int}} = (N-1)|\langle U\rangle_T|/2$ is the mean interaction energy per particle and N represents the number of atoms per lattice site. $\langle U\rangle_T$ characterize the strength of two-body interactions and depends both on the confinement volume and temperature as [17]: $\langle U\rangle_T \approx u\vartheta(\frac{\hbar\omega_X}{k_BT_X})\vartheta(\frac{\hbar\omega_Y}{k_BT_Y})\tilde{\vartheta}(\frac{\hbar\omega_Z}{k_BT_Z})$ with $u = 4a_{eg}^-\sqrt{\frac{m\omega_X\omega_Y\omega_Z}{\hbar}}$, a_{eg}^- the singlet $^1S_0 - {}^3P_0$ scattering length [6] and ϑ and $\tilde{\vartheta}$ functions characterizing the temperature dependence, $\vartheta(x \gg 1) \sim 2\tilde{\vartheta}(x \gg 1) \rightarrow 1$ and $\vartheta(x \ll 1) \sim \tilde{\vartheta}(x \ll 1) \rightarrow \sqrt{x}$.
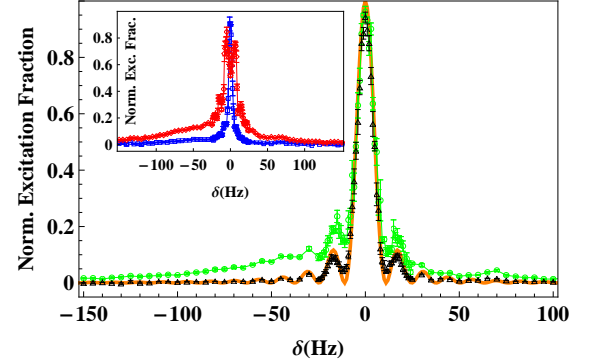

FIG. 2: (Color online) Measured Rabi lineshapes for g to e interrogation (normalized with respect to peak height). The main Panel shows lineshapes taken in a 1D lattice (black triangles) and in a 2D lattice (connected green circles) when the transition is excited with a π-pulse with 80 ms duration. The noninteracting, homogeneous Rabi lineshape for an 80 ms π-pulse is also shown (orange line). The inset shows lineshapes measured in a 2D lattice using a 160 ms 2π-pulse (connected red diamonds) and a 160 ms π-pulse (connected blue squares). Each lineshape was measured under the trapping and temperature conditions described in the main text. The data from each lineshape is collected into bins 1-5 Hz wide.

Using the experimental trapping conditions and temperatures and assuming a moderate $a_{eg}^- = -70a_0$ (a_0 the Bohr radius), we obtain $\gamma^{2D} \sim 10$ in the doubly occupied sites at the center of the 2D lattice. On the contrary, for the central pancake of the 1D lattice with a mean number of 17 atoms and the same scattering length, γ is reduced to $\gamma^{1D} \sim 0.6$. Based on these values, one predicts the development of ISB only in the 2D lattice geometry, a prediction confirmed by our measurements. We measured a series of lineshapes in the 1D and 2D lattices. In the 2D lattice case we also varied the pulse area and Rabi frequency. The resulting data are shown in Fig. 2. To remove some of the statistical noise we performed multiple scans across the transition resonance under each experimental condition. For each scan, the drift of our ultra stable

laser was canceled to <50 mHz per second, and the laser was stepped by 2 Hz each experimental cycle (~1.5 sec). The center of each scan was determined by a fit to a Lorentzian. Each data set consists of ~20 concatenated scans and the direction of the scan was alternated to reduce systematic effects due to residual drift. We separated the data into bins and calculated the mean and standard error of the mean for each bin. At our $4-5\ \mu K$ temperatures, the ISB in the 2D lattice are noticeable but broad. To improve resolution, we reflect the binned line-shape at positive δ (free of ISB when $a_{eg}^- < 0$) and subtract it from the corresponding bin at negative δ (See Fig. 4).

The presence of ISB in the tightly confined geometry can be understood quantitatively by considering an isolated tube with N atoms. We characterize the tube dynamics by defining a set of effective spin operators, $S_{n_j}^{x,y,z}$, in the $\{e,g\}$ basis [1, 11]. Here the subscript n_j is drawn from a fixed set $\vec{n} = \{n_1, n_2 \dots n_N\}$ of initially populated vibrational modes along $\hat{Z}$. The description of the system in terms of effective spin operators is valid provided those initially populated modes remain singly occupied by either a g or an e atom during the excitation process. In the rotating frame, the Hamiltonian of the system up to constant terms becomes [11],

$$\frac{\hat{H}_{\vec{n}}^S}{\hbar} = -\delta S^z - \sum_{j=1}^{N} \Omega_{n_j} S_{n_j}^x - \sum_{j' \neq j}^{N} \frac{U_{n_j, n_{j'}}}{2}(\vec{S}_{n_j} \cdot \vec{S}_{n_{j'}} - \frac{1}{4}). \quad (1)$$

$S^{z,x} = \sum_{j=1}^{N} S_{n_j}^{z,x}$ are collective spin operators. The quantity $U_{n_j,n_{j'}} = u\vartheta(\frac{\hbar\omega_X}{k_B T_X})\vartheta(\frac{\hbar\omega_Y}{k_B T_Y})I_{n_j,n_{j'}}$ measures the strength of the interactions between two atoms in the antisymmetric electronic state. $I_{n_j,n_{j'}}$ is an overlap integral between harmonic oscillator modes along $\hat{Z}$ [17]. Only the $\hat{Z}-$mode distribution is treated exactly since at current temperatures only a few transverse excited modes are populated. The population of transverse modes is accounted for as a renormalization of the interaction parameter.

The interaction part of the Hamiltonian is diagonal in the collective spin basis $|S, M\rangle$, $S = 0(\frac{1}{2}), \dots, N/2$ and $|M| \leq S$. For $N = 2$, the spin basis is spanned by the triplet states $|1, M\rangle$ and the singlet $|0, 0\rangle$. Among the collective states only the $S = N/2$ states are noninteracting. States with $S < N/2$ experience a finite interaction energy. In the presence of excitation inhomogeneity, S is no longer conserved and during excitation of the clock transition, atoms can be transferred mainly between $S = N/2$ and $S = N/2-1$ states. The $N-1$ collective excitation modes $|S = N/2 - 1, M = N/2 - 1, q\rangle$ ($q = 1, \dots N - 1$) with energies $U_{\vec{n}}^{q,N}$ can be accessed from the initially g-polarized state $|N/2, -N/2\rangle$ using $\delta \sim U_{\vec{n}}^{q,N}$. They give rise to $N - 1$ sidebands in the lineshape (Fig. 3):

$$N_{\vec{n}}^e(t,\delta) \approx Nf(t, \delta, \bar{\Omega}_{\vec{n}}) + \sum_{q=1}^{N-1} f(t, \delta - U_{\vec{n}}^{q,N}, \Delta\Omega_{\vec{n}}^{q,N}) \quad (2)$$

with $f(t, \delta, y) \equiv \frac{y^2}{y^2+\delta^2} \sin^2\left(\frac{t\sqrt{y^2+\delta^2}}{2}\right)$ and $\Delta\Omega_{\vec{n}}^{q,N} =$

$2\sum_j \Omega_{n_j}\langle N/2, N/2|S_j^x|N/2-1, N/2-1, q\rangle$. The first term is associated with the carrier and the second with the ISB. For the case $N = 2$, we have $U_{\vec{n}}^{1,2} = U_{\vec{n}}$ and $\Delta\Omega_{\vec{n}}^{1,2} = \Delta\Omega_{\vec{n}}$.

At quantum degeneracy, only the lowest lying vibrational modes need to be considered $\vec{n} = \{0, 1, \dots N - 1\}$. In this case, the interaction sidebands are very narrow. Assuming $t = s\pi/\Omega^B$, with s a numerical constant that describes the pulse duration, the peak width is just $2\Omega^B/s$. Measuring the interaction sidebands thus precisely determines a_{eg}^- and characterizes the $S = N/2 - 1$ spectrum, which has structure for $N > 2$. Since the peak height of the interaction sidebands scales as η_Z^4, large probe inhomogeneities are required to observe them at low temperature.
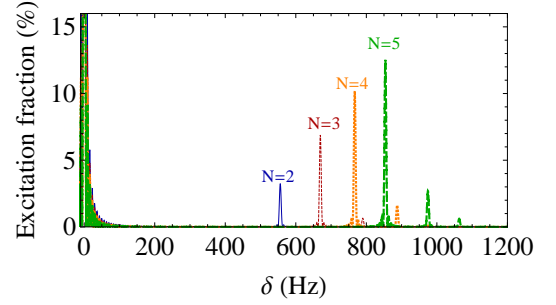

FIG. 3: (Color online) Excitation fraction vs. δ at $T = 0$ for lattice sites with $N = 2 - 5$ atoms. The ISB reveal the $S = N/2 - 1$ spectrum and can be used to probe occupation number in a lattice. The parameters used for the plot were $\eta_Z = 0.4$, $\Omega^B = 2\pi \times 5$ Hz, $t = 1.5\pi/\Omega^B$ and $u = 2\pi \times 2800$ Hz.

In Ref. [9], interaction-dependent transition frequency shifts in RF spectroscopy were used to spectroscopically distinguish sites with different occupation numbers, revealing the shell structure of the Mott insulator phase. The g and e states in AEA have no hyperfine structure, and hence RF spectroscopy is not applicable. However, as shown in Fig. 3, the optical analog of RF spectroscopy– the ISB spectroscopy – can distinguish sites with different atom numbers. This capability can have important implications in quantum simulation [6] and information proposals [4] with AEA.

At finite T, instead of a fixed set of populated modes, a thermal average should be taken. For simplicity and to correspond to our current experiment, we focus on the $N = 2$ case. After evaluating the thermal average [17], we obtain the following approximate expression for the ISB, valid in the regime $|\delta| \gg \Omega^B$, $k_B T_Z > \hbar\omega_Z$ and $t = s\pi/\Omega^B \ll \langle \Delta\Omega \rangle_{T_Z}^{-1}$ (These conditions are satisfied in our experiment):

$$\langle \hat{N}^e \rangle_T \approx \frac{\eta_Z^4 \pi^2 \sqrt{\pi} s\Omega^B}{2|\langle U \rangle_T|}\left(\frac{\hbar\omega_Z}{k_B T_Z}\right)^{-2}\left(\frac{\langle U \rangle_T}{\sqrt{\pi}\delta}\right)^7 e^{-\left(\frac{\langle U \rangle_T}{\sqrt{\pi}\delta}\right)^2}. \quad (3)$$

Fig. 4 shows comparisons between the measured ISB and theoretical curves calculated using Eq. (3). In the 2D lattice, sites near the wings of the lattice beams' Gaussian intensity profiles are significantly shallower than near the center of the beam intersection region, i.e $\omega_\perp(X, Y) \approx$
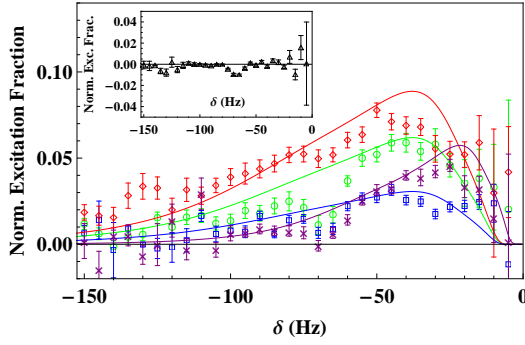
FIG. 4: (Color online) Finite temperature ISB in a 2D lattice (g to e): Symbols correspond to experimental data obtained after reflecting the binned lineshape at positive detuning (free of ISB) and subtracting it from the corresponding bin at negative detuning. Data conditions previously shown in Fig. 2 are displayed with the same symbols and colors. The data indicated by purple crosses corresponds to an 80 ms π-pulse but with different trapping conditions ($\omega_{X,Y,Z} = 2\pi \times \{92, 60, 0.6\}$ kHz at trap center, $T_{X,Y,Z} \sim \{2.5, 2.5, 7.2\}$ μK). The inset shows the absence of ISB in a 1D lattice. Solid curves correspond to theoretical predictions. The dip at $\delta \sim -70$ Hz in the measured ISB is due to residual $m_I = 7/2$ atoms.

$\omega_\perp(0,0)\mathrm{Exp}\left[-(X^2 + Y^2)/W_\perp^2\right]$, with $\omega_\perp \equiv \sqrt{\omega_X \omega_Y}$ and $W_\perp \equiv \sqrt{W_X W_Y} \sim 30$ μm the mean beam waist. This implies u varies from tube to tube; so to compare with experiment, it is important to average Eq. (3) over the populated tube distribution. We assume a uniform distribution of doubly occupied tubes. With this procedure, we obtain lineshapes that reproduce the experimental data if we use $a_{eg}^- = -280a_0$ and $\eta_Z \sim 0.07(0.05)$ for the $\omega_\perp = 2\pi \times 87(73)$ kHz cases. The value of a_{eg}^- that fits the experimental data is outside the range of effective scattering lengths $a_{eg}^{-*} \sim -(35 - 50)a_0$ reported in Ref. [1]. However the discrepancy is attributed to the fact that a_{eg}^{-*} in Ref. [1] corresponded to the effective scattering length required to model the entire lattice array by a single tube at the trap center, and thus $|a_{eg}^{-*}|$ should be smaller than $|a_{eg}^-|$. In agreement with theory, the ISB's position and width are on the order of $\langle U \rangle_T$ and their resonant peak heights (normalized to the carrier) decrease with decreasing Ω^B and increase with pulse area $s\pi$.

We determine the nuclear spin purity of the atomic sample to be $> 97\%$ by scanning the probe laser over the clock transition frequencies for other nuclear spin states. The signature of the remaining 3% is the small resonant peak at $\delta \sim 70$ Hz in Fig. 2. By comparing the amplitude of this small peak with the ISB, we conclude that the observed sidebands are not caused by s-wave collisions between unpolarized atoms.

We also performed e to g Rabi interrogation by first transferring all the atoms from g to e with a resonant pulse, then removing the remaining g atoms and finally interrogating the e atoms with an 80 ms π-pulse. However, even under tightly confined conditions we did not see evidence of ISB in this case. The lack of ISB can be attributed to the absence of double occupancy in a single tube due to p-wave inelastic $e - e$ two-body losses (during the relevant experimental time

scale), similar to the ones recently measured in ultracold KRb molecules [15] and ^{88}Sr atoms (s-wave) [16].

The effect of tunneling between tubes could in principle modify the shape and height of the ISB (but not its mean position) and generate an additional frequency shift of the carrier. The latter can be particularly relevant in the strongly interacting regime where collisional shifts would otherwise be suppressed. In order to investigate the effect of tunneling, we also took one set of data under conditions which reproduced those used in Ref. [1]. The presence of ISB in this lineshape, measured with $T_{X,Y} \sim 2.5$ μK (see Fig. 4), completely rules out the possibility that these spectroscopic features are caused by tunneling since, under these conditions, we predict that tunneling rates are suppressed by two orders of magnitude compared to $T_{X,Y} \sim 4.5$ μK.

———

[1] M. D. Swallows et al., Science 331, 1043 (2011); G. K. Campbell et al., Science 324, 360 (2009).

[2] N. D. Lemke et al., Phys. Rev. Lett. 103, 063001 (2009); A. D. Ludlow et al., Science 319, 1805 (2008); T. Akatsuka, M. Takamoto and H. Katori, Nat. Phys. 4, 954 (2008); G. K. Campbell et al., Metrologia 45, 539-548 (2008); J. Ye, H. J. Kimble and H. Katori, Science 320, 1734 (2008); M. M. Boyd et al., Phys. Rev. Lett. 98, 083002 (2007).

[3] C. W. Chou et al., Science 329, 1630 (2010).

[4] D. Hayes, P. S. Julienne, and I. H. Deutsch, Phys Rev. Lett. 98, 070501 (2007); A. J. Daley et al., Phys. Rev. Lett. 101, 170504 (2008); A. V. Gorshkov et al., Phys. Rev. Lett. 102, 110503 (2009); I. Reichenbach, P. S. Julienne, and I. H. Deutsch, Phys. Rev. A 80, 020701 (2009).

[5] B. J. DeSalvo et al., Phys. Rev. Lett. 105, 030402 (2010); M. K. Tey et al., Phys. Rev. A 82, 011608 (2010); S.Taie et al., Phys. Rev. Lett. 105, 190401 (2010).

[6] A. V. Gorshkov et al., Nature Physics 6, 289 (2010); M. A. Cazalilla, A. F. Ho, and M. Ueda, New J. Phys. 11, 103033 (2009); M. Hermele, V. Gurarie, and A. M. Rey, Phys. Rev. Lett. 103, 135301 (2009); M. Foss-Feig, M. Hermele, and A. M. Rey, Phys. Rev. A 81, 051603(R) (2010).

[7] T. C. Killian et al., Phys. Rev. Lett. 81, 3807 (1998).

[8] S. Giorgini, L. P. Pitaevskii and S. Stringari, Rev. Mod. Phys. 80, 1215 (2008).

[9] G. K. Campbell et al., Science 331, 369 (2006).

[10] K. Gibble, Phys. Rev. Lett. 103, 113202 (2009).

[11] A. M. Rey, A. V. Gorshkov, and C. Rubbo, Phys. Rev. Lett. 103, 260402 (2009).

[12] D. J. Wineland and W. M. Itano, Phys. Rev. A 20, 1521 (1979).

[13] H. Häffner et al., Phys. Rev. Lett. 90, 143602 (2003).

[14] S. Blatt et al., Phys. Rev. A 80, 052703 (2009).

[15] S. Ospelkaus et al., Science 327, 853 (2010).

[16] Ch. Lisdat et al., Phys. Rev. Lett. 103, 090801 (2009)

[17] See supplemetary information.